IEEE Photonics Journal
An IEEE Photonics Society Publication

Practical Materials Chemistry Approaches for Tuning Optical and Structural Properties of Group IV Semiconductors and Prototype Photonic Devices

Volume 2, Number 6, December 2010

J. Kouvetakis
J. Mathews
R. Roucka
Andrew V. G. Chizmeshya
J. Tolle
J. Menendez

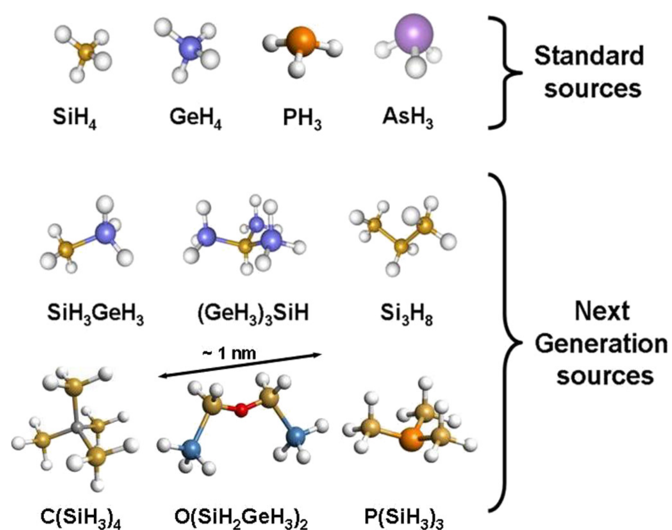

DOI: 10.1109/JPHOT.2010.2081357
1943-0655/$26.00 ©2010 IEEE

IEEE photonics SOCIETY
IEEE

Practical Materials Chemistry Approaches for Tuning Optical and Structural Properties of Group IV Semiconductors and Prototype Photonic Devices

J. Kouvetakis,[1] J. Mathews,[1,2] R. Roucka,[1] Andrew V. G. Chizmeshya,[1] J. Tolle,[1] and J. Menendez[1]

[1]Department of Chemistry and Biochemistry, Arizona State University, Tempe, AZ 85287 USA
[2]Department of Physics, Arizona State University, Tempe, AZ 85287 USA

DOI: 10.1109/JPHOT.2010.2081357
1943-0655/$26.00 ©2010 IEEE

Manuscript received September 1, 2010; revised September 20, 2010; accepted September 21, 2010. Date of publication September 27, 2010; date of current version October 15, 2010. This work was supported by the U.S. Air Force under Contract DOD AFOSR FA9550-06-01-0442 (MURI program), by the U.S. Department of Energy under Contract DE-FG36-08GO18003, and by the National Science Foundation under Grant DMR-0907600. Corresponding author: A. V. G. Chizmeshya (e-mail: chizmesh@asu.edu).

Abstract: We report new approaches based on rational design and preparation of chemical vapor deposition precursors involving novel main-group hydrides to fabricate new families of Si-based semiconductors and prototype devices that display compositional and structural inheritance, from the parent molecule to the solid end product. This methodology enables materials synthesis at extraordinarily low temperatures that are compatible with complementary metal-oxide-semiconductor (CMOS) processing/selective growth and provides the means for obtaining highly metastable strain states in prototype structures that cannot be obtained by conventional protocols. Some of the materials and devices under development, involving alloys in the Si–Ge–Sn system, open up exciting opportunities in photodetectors and photovoltaics because they grow directly on cheap Si substrates and cover an extended range of the near-infrared spectrum that is not accessible to current photovoltaic and optoelectronic group IV semiconductors.

Index Terms: Germanium, Si-based optoelectronics, photodetectors, near infrared.

1. Introduction

Modern semiconductor synthesis and processing predominately relies on the use of simple inorganic hydrides—including the prototypical compounds GeH_4, SiH_4, B_2H_6, AsH_3 and PH_3—which are currently considered to be the industry standards. Higher order analogs $(Si_2H_6, Si_3H_8, Ge_2H_6)$, previously regarded as esoteric or commercially inaccessible, have also been developed and are now used in mass production. In fact, a range of technical problems identified in the International Technology Roadmap for Semiconductors are being addressed using sources such as Si_3H_8. As the demand continues for improved semiconductor devices, the search for new synthetic chemistries and associated processes has dramatically intensified. In this context, hydride precursors remain the preferred vehicle for pursuing exploratory research as well as commercial fabrication of a wide range of novel solid-state materials and practical device architectures. Compared with conventional metalorganic chemical vapor deposition (MOCVD) sources, these compounds are generally more volatile and devoid of metal-organic functionalities that can incorporate carbon

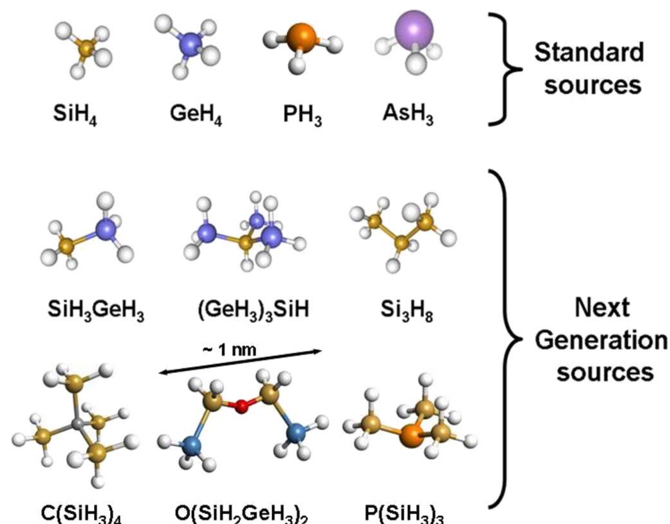

Fig. 1. Conventional and "next generation" molecular hydrides used in various film depositions. Carbon (dark gray); oxygen (red); silicon (yellow); germanium (blue); phosphorous (orange); and hydrogen (white).

impurities into the final product, thereby degrading device performance. On the other hand, the weakly bonded H ligands are readily eliminated as highly stable, noncorrosive H_2, leaving groups leading to the highest possible purity in the final product at extraordinarily low temperatures that are well below the typical desorption range of H atoms in conventional CVD of semiconductors [1]. Accordingly, the latter may serve as surfactants in the epitaxy-driven crystal assembly of materials possessing fundamentally incompatible surface energies. Our work to date provides mounting evidence that this metastable regime is responsible for the layer-by-layer growth of perfectly uniform and atomically flat heterostructures suitable for the development of thick device quality films. Most importantly, this low-temperature nontraditional processing is perfectly compatible with the fabrication of thermally sensitive device structures in typical back-end complementary metal-oxide-semiconductor (CMOS) processes.

Ironically, the relatively low thermal stability and high reactivity of the hydride compounds, both of which are advantageous from a materials synthesis perspective, have hindered their production and widespread deployment [2]. To overcome this limitation, our team at Arizona State University (ASU) has developed, over the course of the past decade, an extensive portfolio of purpose-built hydrides comprised of main-group elements. Our approach is based on molecular designs intended to improve stability and/or tractability, giving synthetic access to many more compounds that can be isolated and manipulated at room temperature. For example, an entire class of previously unknown azido-alanes and -gallanes has been produced, including the simple and highly versatile H_2GaN_3, D_2GaN_3, $H(Cl)GaN_3$, $H(Br)GaN_3$, and $(H_2AlN_3)NMe_3$ complexes [3]–[5]. These have provided new pathways to form nitrides at conditions that are inaccessible by conventional MOCVD for the purpose of integration with Si electronics:

$$H_2GaN_3 \rightarrow H_2 + N_2 + GaN. \quad (1)$$

Other recent materials synthesis work [6]–[12] using single source precursors, containing C, N, O, P, As, and Sb centers bonded to silyl (SiH_3) and germyl (GeH_3) ligands, has identified an extensive and diverse sequence of molecules including the previously known SiH_3CN, GeH_3CN, $O(SiH_3)_2$, $N(SiH_3)_3$, $C(SiH_3)_4$, $C(SiClH_2)_4$, $C(GeH_3)_4$, $SiH_3NCNSiH_3$, $SiH_3C_2SiH_3$, $P(GeH_3)_3$, $As(GeH_3)_3$, $P(SiH_3)_3$, or newly prepared $O(SiH_2GeH_3)_2$ derivatives (see Fig. 1). These have been demonstrated to exhibit tunable reactivities, stoichiometries and bonding arrangements that enable the synthesis of

new electronic and structural materials, including metastable alloys and compound semiconductors as well as superhard and ultrastrong ceramics based on light elements. The synthesis protocols are diverse and may involve unimolecular decompositions, simple reactions between molecules, or interaction between molecules and atomic beams. For example, the combination of SiH_3CN with Al atoms yields SiH_3CN:Al transient intermediates [see (2) below], which in turn eliminate robust H_2 to produce stoichiometric SiCAlN quaternaries with direct band gaps [6]

$$\mathrm{SiH_3CN} + \mathrm{Al(gas)} \rightarrow \text{“}\mathrm{SiH_3CN{:}\ Al}\text{”} \rightarrow \mathrm{SiCNAl(crystal)} + 3/2\mathrm{H_2}. \quad (2)$$

In this case, it was found that the intact incorporation of the Si-C-N nanoscale cores provides a mechanism to control the hexagonal poly-type stacking in the structure and, in turn, the associated fundamental *band gap*. In a related study the reaction of $O(SiH_3)_2$ or $P(SiH_3)_3$ with NH_3 produces perfectly stoichiometric Si_2N_2O or Si_3N_3P dielectrics [see (3) below], respectively, with immediate applications in on-chip-capacitors. Here, again, the resultant solid condenses directly on the Si substrate surface by low temperature assembly of Si-O-Si or P-Si_3 nanofragments derived from the parent molecules [7], [8]

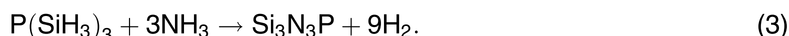

$$\mathrm{P(SiH_3)_3} + 3\mathrm{NH_3} \rightarrow \mathrm{Si_3N_3P} + 9\mathrm{H_2}. \quad (3)$$

The simplest possible protocol to new materials synthesis involves single-source thermal dehydrogenation reactions on structurally suitable platforms. Using this technique, we have successfully produced semiconductors of composition Ge_4C and Si_4C via complete H_2 elimination from $C(GeH_3)_4$ and $C(SiH_3)_4$, respectively [11], [12]. In both cases, the intact incorporation of the Si_4C/Ge_4C tetrahedral units into the solids leads to a unique sub-lattice in which all carbon atoms are ordered as third nearest neighbors. We note, that these kinetically stabilized configurations, which are typically created heteroepitaxially on Si via UHV-CVD, are not thermodynamically accessible via standard near-equilibrium synthetic methodologies based on traditional molecular sources. Collectively the above examples show that the compositional and structural inheritance from the parent molecule to a solid end product is a general and powerful concept with great potential for future innovations in functional materials design and discovery.

The precursor-driven synthesis approach has been extensively used to demonstrate the generalized low-temperature deposition of alloys and strained-layer heterostructures in the SiGe, GeSn, SiGeSn, SiSn, and SiGeSn/Ge systems [13]. The application of this technique enables fabrication of novel devices such as extended-range near-IR GeSn photodiodes fully compatible with Si processing protocols using silicon as a universal platform. Notable breakthroughs for this class of systems have been described in our prior work. In this paper, we present our most recent advances with special focus on the following topics: (a) precise nanoscale control of composition and morphology in Ge-rich $Si_{1-x}Ge_x$ materials with strained engineered structures [14]–[16], (b) fabrication of Si–Ge–Sn materials which serve as active layers and/or enabling buffers for Si integration in IR optoelectronics/photonics [17]–[20], and (c) new routes to device-quality Ge on Si for applications in detectors and multijunction photovoltaics [21]. In each of the above areas, we first provide *methodologies, introduce background information*, and then describe key new results.

The CMOS compatible fabrication of these systems was made possible by a new generation of Si–Ge–Sn hydrides and corresponding derivatives of group V dopant atoms. From a structural and bonding perspective these precursors incorporate molecular cores with precisely tailored nearest and second neighbor configurations that ultimately define the properties of the synthesized semiconductor alloys. This approach also addresses constraints in device fabrication such as the need for both selective area growth, limited processing temperatures, and *in situ* doping of metastable semiconductors leading to full activation at high carrier concentrations. It has also added significant momentum to the emergence of silicon photonics—a new and thriving area in optical materials science and engineering [22].

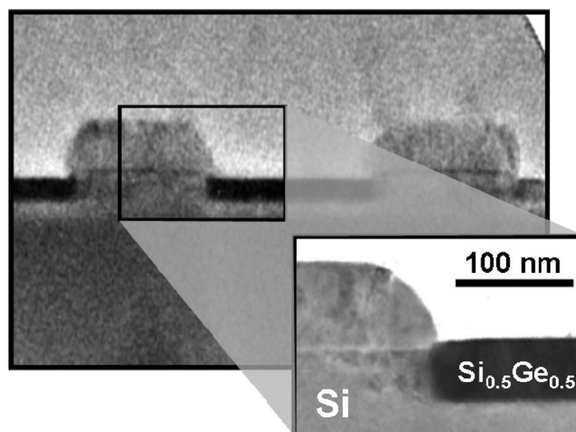

Fig. 2. XTEM micrograph showing selective growth of SiGe in the "source" and "drain" areas of a device via deposition of silyl germanes. Note the smooth and continuous morphology devoid of threading defects. The enlarged view indicates the absence of any deposition on nitride spacers or on the polysilicon gate.

2. Results and Discussion

2.1. Designer Precursor Approaches to Strained-Engineered, Ge-rich $Si_{1-x}Ge_x$

The key Si_xGe_y building blocks of these materials are obtained from a broad-range of previously unknown germyl-silane hydrides containing direct Si-Ge bonds. Recent examples include the subset of deposition precursors with the general formula $(H_3Ge)_xSiH_{4-x}(x = 1 - 4)$, suitable for growth of thin $Si_{1-x}Ge_x$ films with a wide range of Ge contents at low temperatures under processing conditions inaccessible with currently available chemical precursors, notably germane gas and silanes [14]. $Si_{1-x}Ge_x$ alloys are utilized in vital components of computer chips, solar cells, and other semiconductor devices. In the case of logic chips, the materials already play a critical role in strained silicon technologies, enabling the continued pursuit of Moore's law for performance improvements. The $(H_3Ge)_xSiH_{4-x}$ compounds were initially synthesized at ASU and were subsequently used to fabricate $Si_{1-x}Ge_x$ advantageously. This work in turn led to the discovery of new branches within the general silyl-germyl class including butane-like analogs such as $GeH_3SiH_2SiH_2GeH_3$, $GeH_3GeH_2SiH_2GeH_3$ and chlorinated derivatives [15]. The specialized processing requirements and deposition behavior of selected compounds was also demonstrated. In addition to fundamental value, recent collaborations with Voltaix Corporation and ASM America have determined that they are also useful for industrial applications and can be manufactured economically [23].

Our inventory of germyl-silane precursors was subsequently expanded to include the chlorinated $Cl_nH_{6-n}SiGe$ hydrides. Selectively controlled chlorination of H_3SiGeH_3 is provided by reactions with BCl_3 to produce ClH_2SiGeH_3 and $Cl_2HSiGeH_3$ and poly-substituted derivatives according to the following equation [16]:

$$nBCl_3 + 3H_3SiGeH_3 \rightarrow n/2B_2H_6 + 3Cl_nH_{6-n}SiGe. \quad (4)$$

This scheme represents a viable single-step route to the target compounds in practical yields for industrial level semiconductor applications, particularly once the starting SiH_3GeH_3 material is produced on a commercial scale by Voltaix. Higher order polychlorinated derivatives such as $Cl_2SiHGeH_2Cl$, $Cl_2SiHGeHCl_2$, $ClSiH_2GeH_2Cl$ and $ClSiH_2GeHCl_2$ were also obtained in semiconductor grade purity. The built-in Cl functionalities of these compounds are specifically designed to facilitate selective growth compatible with CMOS processing. In particular, low-temperature epitaxy (380–430 °C) produces stoichiometric SiGe films seamlessly, conformally, and selectively in the recessed regions of prototypical device structures, as seen in Fig. 2. The materials deposited via

this method exhibit monocrystalline microstructures, smooth and continuous surface morphologies, reduced defect densities, and record high compressive strains.

The synthetic "palette" of chlorinated SiGe was most recently extended to the Ge-rich propane- and butane-like family of molecules including $SiH_2(GeH_3)_2$, $SiH(GeH_3)_3$, and $(SiH_2)_2(GeH_3)_2$ by selective chlorination of their -SiH_2, -SiH, and -SiH_2-SiH_2- bridging ligands. This approach led to pure compounds such as $ClHSi(GeH_3)_2$, $Cl_2Si(GeH_3)_2$, $ClSi(GeH_3)_3$, and $ClHSiSiH_2(GeH_3)_2$ [24]. The dichlorinated butane-like species $(ClHSi)_2(GeH_3)_2$ and $Cl_2SiSiH_2(GeH_3)_2$ are also obtained as isomeric mixtures and embody a new class of highly reactive single source precursors that are of fundamental and practical interest. Depositions of the more reactive $ClHSi(GeH_3)_2$ analog in this class produced $Si_{0.33}Ge_{0.67}$ layers with novel epitaxy-stabilized tetragonal structures exhibiting unprecedented compressive strain approaching -2.4%. This is $\sim$90% of the maximum value (2.75%) expected for this composition and it is obtained in film thicknesses of 20–25 nm that far exceed the equilibrium critical value (< 2 nm) of the same material grown pseudomorphically on Si(100). The external stress required to achieve this deformation in free standing samples is $\sim$4 GPa which underscores the extreme strain state achieved in these films. XTEM observations of this material reveal a uniform thickness, a smooth surface and fully commensurate interfaces. Furthermore, diffraction contrast analysis indicates that the layers are largely free of threading defects.

The above examples demonstrate that a single source route enables facile conversion of diamond cubic Si-Ge into tetragonally structured alloys with average lattice constants of 5.451 Å and 5.688 Å that cannot be obtained by conventional methods. In this case, fully stressed $Si_{0.50}Ge_{0.50}$ layers with lattice parameters of 5.428 Å and 5.595 Å and thickness of 60 nm are grown pseudomorphically on Si via decomposition of SiH_3GeH_3. Accordingly, this approach may represent a practical strategy for stress engineering and control which could lead to significant performance gains by enhancing the mobility in *p*-type metal-oxide-semiconductor device channels. Additionally, it circumvents the need for the usual multicomponent reactions and corrosive Cl_2 etchants necessary to promote selective, strained-layer deposition in conventional processes.

2.2. Materials and Device Development in the Ge and Ge-Sn Systems

Most recently, the theme of precursor driven approach was extended to the arena of activation of group IV semiconductors where effective *n*-doping has been traditionally very difficult to achieve by conventional physical and chemical methods including implantation of solid sources and vapor deposition of PH_3 and AsH_3 molecules. In our work, donor incorporation and activation is achieved efficiently *in situ* using an entire series of newly introduced single source precursors containing P, As, and Sb centers bonded to silyl (SiH_3) and germyl (GeH_3) ligands such as $P(SiH_3)_3$, $P(GeH_3)_3$, $As(GeH_3)_3$, and $Sb(GeH_3)_3$. For example, the $(SiH_3)_3P$ compound was used to co-dope germanium with Si and P for the first time by building a prototype p^{++}Si(100)$/i-$Ge$/n$-Ge photodiode structure [25]. The resultant *n*-type Ge layers contained active P carrier levels of $\sim 5 \times 10^{19}$ and Si concentrations of $\sim 10^{20}$ atoms/cm^3 which is within the range expected for incorporating the entire Si_3P units into the diamond cubic Ge matrix. Extensive characterizations for structure, morphology, and crystallinity indicate that the Si "co-dopant" plays essentially a passive role and does not compromise the device quality of the host material, nor does it fundamentally alter its optical properties. In Fig. 3, XTEM and atomic force microscopy (AFM) images show that *the* surface of the film is atomically flat and the bulk is virtually free of threading dislocation except for the interface region which reveals the typical "pile up" of defects within 50 nm above the Ge/Si(100) heterojunctions. From a broader device design and fabrication perspective the $(SiH_3)_3P$ precursor could also offer a simple and effective route to Ge superdoping for possible application in electrical contact design or even superconductivity.

As in the case of $P(SiH_3)_3$, the analogous Ge compounds $P(GeH_3)_3$ and $As(GeH_3)_3$ have also been specifically designed to deliver intact Ge_3P and Ge_3As *near-tetrahedral* cores into the lattice sites of the diamond-cubic structures at low temperatures (see Fig. 4). In recent device applications, this precursor method has proven to be far superior to current state-of-the-art approaches for *n*-type

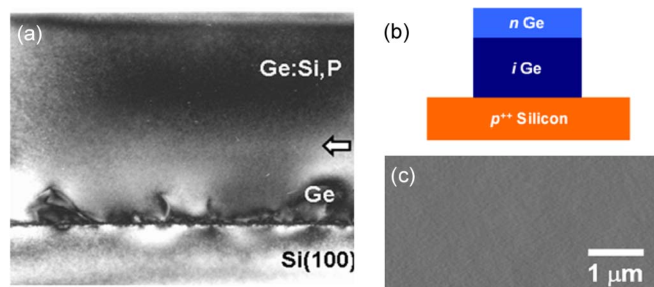

Fig. 3. (a) XTEM micrograph of a 700-nm-thick Ge/GeSiP film, which appears to be flat and free of penetrating defects. Arrow indicates the switchover point in the growth of the intrinsic Ge layer to the P/Si co-doped overlayer. The microstructure at the growth transition region is continuous and indistinguishable from that of the bulk. (b) Schematic of the prototype $p-i-n$ heterostructure. (c) AFM image indicating an RMS roughness of $\sim$0.19 nm for the 5×5 μm^2 areas [25].

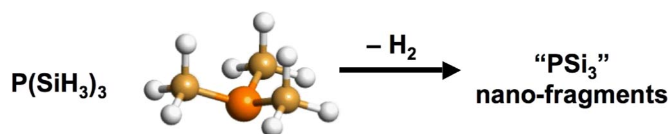

Fig. 4. Dehydrogenation reaction of $P(SiH_3)_3$ producing PSi_3 near tetrahedral molecular cores. These are incorporated into the diamond lattice ensuring full activation of the P atoms at low temperatures without clustering or segregation.

doping utilizing arsine and phosphine which tend to significantly reduce the growth rates due to complicated surface reactions at the growth front [26]–[28]. The use of the latter compounds containing relatively strong P-H and As-H bonds are also known to require high temperature depositions, which leads to clustering, precipitation, and surface segregation of the dopants, thereby inhibiting the formation of compositionally uniform profiles and thus degrading the overall quality of the material [29]. Ultimately, these source- and process-related issues severely limit the active carrier concentrations achievable to levels below the 10^{19} atoms/cm^3 range [30]. While this is acceptable for some applications, such as SiGe modulators [31], much higher levels must be routinely attained to fabricate Si–Ge–Sn photodetectors, as well as Ge-based lasers for applications in the general area of Si-photonics. In this regard, the $P(GeH_3)_3$ compound is particularly useful in CMOS compatible fabrication of high-performance $Ge_{0.98}Sn_{0.02}$ $p-i-n$ photodetectors integrated directly on Si platforms [32]. The PGe_3 cores of the precursor are incorporated intact into the host GeSn structure to yield a homogeneous distribution of substitutional P without clustering or segregation, ensuring full activation at concentration levels in the 10^{18} to $10^{20}/cm^3$ range. In contrast to conventional high temperature/energy methods mentioned above, this soft chemistry strategy also mitigates structural and morphological imperfections in the relatively fragile GeSn which ultimately degrade the performance of these devices.

The GeSn alloys used for this application represent a new class of group IV materials that are particularly attractive not only for IR detector but for photovoltaic devices requiring band gaps lower than that of Ge (0.80 eV) as well. Our CVD approach to the growth of these materials directly on Si wafers is based on straightforward reactions of conventional Ge_2H_6 with SnD_4 at low temperatures of 250 to 350 °C. In general we find that over this range there is an inverse relationship between the growth temperature and the amount of Sn incorporated in the alloy. Samples with low Sn content (2%–5%) are routinely grown at 350–330 °C, respectively and have been used to produce prototype devices as discussed below. To produce materials with higher Sn contents the temperature must be systematically and dramatically reduced to ensure full incorporation of the atoms in the structure. For example at 290, 275, 270, and 260 °C, we obtain Sn concentrations of 9, 11, 13, and 15%, respectively. The reduction in temperature is associated with a concomitant decrease in

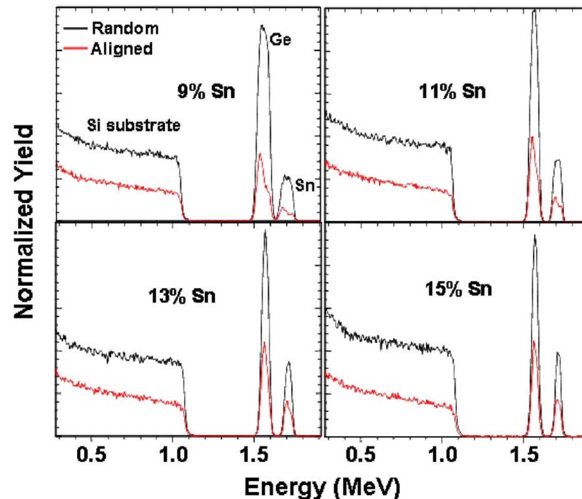

Fig. 5. Aligned and random RBS spectra for a series of $Ge_{1-x}Sn_x$ samples containing 9, 11, 13, and 15% Sn, demonstrating that a similar high degree of Ge and Sn substitutionality is systematically achieved in all films.

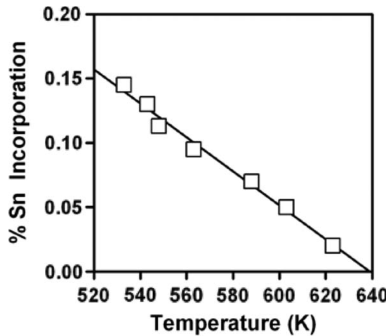

Fig. 6. Amount of Sn incorporation in $Ge_{1-y}Sn_y$ alloy films as a function of growth temperature, indicating an inverse linear relationship over the range 260–350 °C.

growth rate from 20 nm/per minute at 350–370 °C (2% Sn) to 1.5 nm/min at 260 °C (15% Sn). Fig. 5 shows the random and channeled plots acquired from representative samples containing the aforementioned compositions. Notice that the ratio of the random over the aligned peak heights [which is defined as χ_{min} in Rutherford backscattering spectrometry (RBS)] for the Sn and Ge peaks is the same in each sample indicating full substitutionality of both atom types, which is consistent with single phase material.

It is noteworthy that the 260 °C temperature is well beyond the characteristic range for epitaxy driven deposition by CVD reactions involving molecular hydrides of group IV materials. Perhaps more surprising is the fact that hydrogen is fully eliminated from the growth front allowing the formation of supersaturated alloys with single-crystalline structures under highly metastable conditions. Fig. 6 contains a plot of the amount of Sn incorporation in the alloy as a function of growth temperature indicating that an inverse linear relationship exists between the two parameters. This in turn reflects the almost linear concentration increase of the SnD_4 needed to deliver the higher Sn contents while unimolecular decomposition of SnD_4 leading to precipitation of elemental Sn is suppressed at the low temperatures employed in this range.

At the highest growth rates thick and atomically flat films containing 2%–3% Sn have been routinely obtained and are found to possess low densities of threading dislocations ($\sim 10^6/\text{cm}^2$), as required for the fabrication of photodiodes [33]. Even at these modest concentrations, the latter

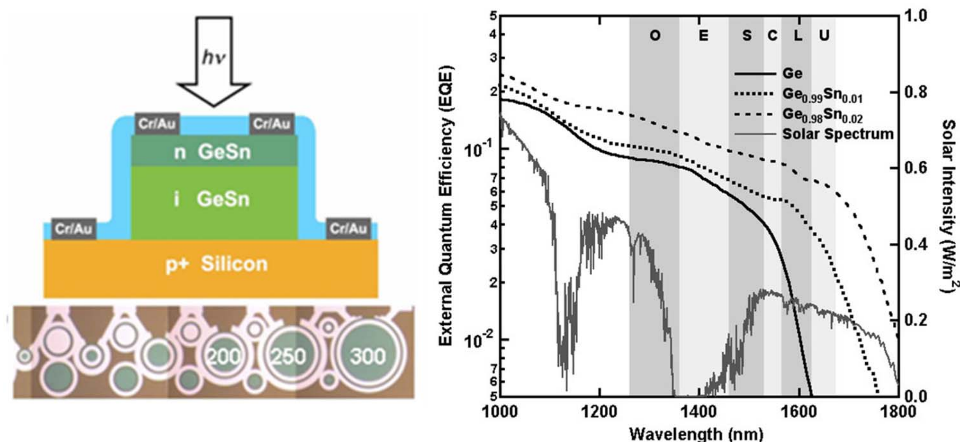

Fig. 7. (Left) Schematic representations of the p-i-n photodiode showing the sequence of the layers and the oxide antireflective coating and the metal contacts. The mask containing the circular mesas with diameters ranging from 60 to 300 is shown below along with the metal contacts of the devices. (Right) External quantum efficiency plots comparing the optical response of ~350-nm-thick $Ge_{0.99}Sn_{0.01}$ and $Ge_{0.98}Sn_{0.02}$ photodiodes with a pure Ge analog. The EQE of the GeSn is significantly higher the entire near IR range due to the higher absorption coefficient of the alloy and the absorption edge shifts systematically to higher wavelength with increasing Sn content. This also allows a significant degree of overlap with the solar spectrum (dark gray trace) within the measured wavelength range [32], [34].

devices are found to posses a significantly extended detection range relative to elemental Ge. Furthermore, extensive optical characterizations of the materials have demonstrated a rapid reduction of the direct absorption edge as a function of Sn content to the extent that only a very small fraction of 2% Sn is sufficient to achieve full coverage of all telecom windows with an absorption coefficient that is at least ten times higher than that of Ge [34]. Accordingly, these materials have a true potential to extend the optoelectronic performance of elemental Ge into the mid infrared region of the spectrum.

The first generation of such diodes based on p^{++}Si(100)$/i-Ge_{1-y}Sn_y/n-Ge_{1-y}Sn_y$ geometries (and $n-i-p$ analogs) were fabricated using the above synthesis and doping protocols involving the highly reactive hydrides Ge_2H_6, SnD_4 and $P(GeH_3)_3$. Subsequent spectral measurements of these devices revealed that the range of their responsivity is dramatically expanded up to at least 1750 nm, well beyond the direct band gap of Ge (1550 nm), indicating a broader coverage of the IR spectrum, as expected [32], [34]. The external quantum efficiency (EQE) plot obtained from of a representative devices with an intrinsic layer thickness of ~350 nm and a mesa size of 300 micrometers in diameter is shown in Fig. 7. The data provide unequivocal evidence that the incorporation of a small amount of Sn (~1–2 at. %) into the Ge significantly extends the detection range of the material, and makes the case that $Ge_{1-y}Sn_y$ alloys represent a practical and potentially superior alternative to Ge for telecommunication applications. In particular, the EQE of this diode over the L band (1565–1625 nm) is about a factor of 2 higher than that of any tensile strain Ge device in the literature confirming the attractive properties of these alloys for detection in this wavelength range. This extended response may also have significant implications for the design of novel photovoltaic devices as shown in Fig. 7, since it makes it possible to capture a portion of the solar spectrum between 1400 nm and 1800 nm that is largely lost in current multijunction solar cells based on Ge as the low band gap component.

The EQE plot of analogous diodes based on pure Ge layers that are grown directly on Si at low-temperatures and processed in a nearly identical manner is also included in Fig. 7. The results confirm the higher responsivity of GeSn despite the significantly lower dark currents measured in the Ge counterparts, as shown in Fig. 8, which compares the data for pure Ge and GeSn devices processed in the same way, and containing essentially identical architectures and layer thicknesses. In fact, the dark currents for our Ge diodes shown here are comparable to those reported for similar devices grown at much higher temperatures, underscoring the high quality of our

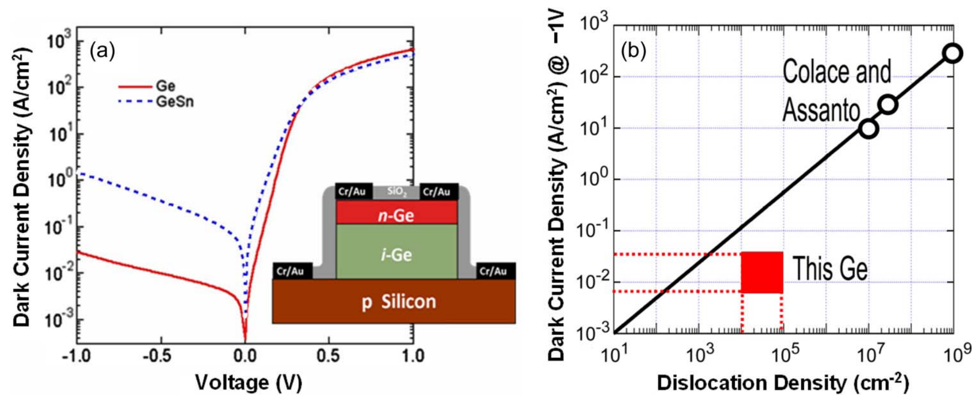

Fig. 8. (a) I–V graphs obtained from Ge and GeSn device mesas with sizes of 100 μm in diameter. The dark current in GeSn is significantly higher than that of pure Ge likely due to either inferior crystallinity or alloy scattering effects. (b) Dark current versus dislocation density trends for Ge-on-Si heterostructure diodes, as determined by Colace and Assanto [36]. The red region indicates the ranges of dislocation density and dark current for samples grown in this study.

specially developed Ge materials in both intrinsic and doped form. The latter were deposited using new synthesis protocols that allow unprecedented control of film microstructure, morphology and purity [35]. The method utilizes designer molecular precursors targeted to tailor the surface reactions at the growth front. The deposition is conducted at 350–420 °C using molecular mixtures of Ge_2H_6 and small amounts of highly reactive $(GeH_3)_2CH_2$ organometallic additives. Under these conditions, gas-phase reactions are suppressed. Optimized molar ratios of these mixtures have enabled layer–by-layer growth. The driving force for this novel reaction mechanism is the facile elimination of extremely stable CH_4 and H_2 byproducts. Our results in general indicate that the additives moderate the surface diffusion of the Ge atoms thereby profoundly altering the classic Stranski-Krastanov growth mechanism of epitaxial Ge on highly mismatched Si surfaces. This approach produces atomically smooth (AFM RMS $\sim$0.2 nm) and stress-free Ge films with dislocation densities less than 10^4 cm^{-2}, as required to advance the optoelectronic performance of the IR photodetectors. An empirical relationship between dislocation density and dark current for Ge-on-Si heterostructure diodes, as determined by Colace and Assanto [36], is shown in the right panel of Fig. 8. The red shaded region indicates the dislocation energy range and dark current range for samples grown in this study, showing a close correspondence with the empirical trend.

We anticipate that our novel CVD approach to the growth and doping of these Ge and GeSn materials/devices should be compatible with the selective growth strategies needed for waveguide photodetectors. In particular, the much higher alloy absorption coefficient of GeSn may actually eliminate the constraints that dictate a waveguide geometry for Ge on Si receivers. We also anticipate that increased Sn concentrations in this alloy should to shift the responsivity further into the infrared, overlapping the wavelength range of InGaAs detectors. From a growth and doping perspective, a critical advantage of our inherently low-temperature soft-chemistry approach is that all high-energy processing steps are completely circumvented.

GeSn quantum wells have been grown using higher gap SiGeSn barrier layers. These materials' architectures have yielded light emission in the vicinity of the direct gap and are considered critical building blocks for a range of novel optoelectronic structures including high-speed modulators based on the quantum-confined Stark effect (QCSE). Most recently, however, we have observed direct-gap photoluminescence at room temperature in thick GeSn layers grown directly on Si, in which confinement effects are not manifest. In this case, we find that the luminescence peak shifts to longer wavelengths as the Sn concentration is increased from $\sim$0.8, 0.73 eV and 0.68 eV for samples containing 0.0 Sn% (pure Ge), 1.5% Sn, and 3.0% Sn, respectively. These peak values very closely follow the direct gap energies obtained from ellipsometric studies of the dielectric function. Preliminary photoluminescence spectra show that while these low-Sn concentration alloys

are expected to be indirect gap semiconductors, the separation between the direct and indirect edges is less than in pure Ge, and therefore, the Γ-valley minimum in the conduction band of the GeSn alloy is easily populated by a combination of photo- and thermal excitation. The indirect gap emission is far more sensitive to defects than the direct gap emission, and therefore, it is not observed in these samples. This is similar to previous results for Ge layers on Si that have led to the recent announcement of lasing in these materials. The advantage of GeSn alloys is that their emission energy is tunable as demonstrated in our studies (to be published). Moreover, the separation between conduction band minima is also tunable, and this reduces (or eliminates altogether) the level of n-type doping needed to achieve lasing devices.

2.3. Si–Ge–Sn System

The previously discussed $Ge_{1-x}Si_x$ alloys have recently been introduced into conventional CMOS to enhance the performance of Si-based transistors and expand the optoelectronic capabilities of group IV materials enabling the design and realization of novel high-speed modulators and quantum cascade lasers [22], [31], [37]–[39]. However, the large lattice mismatch between Si and Ge that enables these strain engineering technologies is also the source of various structural issues. In the case of multijunction photovoltaics, the incorporation of Ge-rich components has *not* been possible due to the high levels of deleterious dislocations created at the mismatched heterojunctions. Furthermore, the band structure and lattice dimensions of $Si_{1-x}Ge_x$ cannot be decoupled since the compositional change needed to adjust the band gap of the alloy produces a simultaneous change in molar volume and, therefore, the lattice constant.

Most recently, the focus in group IV materials has shifted to the Si–Ge–Sn system, where the compatibility in electronegativities and bonding character between the constituents allows rough estimates of band gaps and optical properties to be made using simple Si, Ge and Sn averages. Intriguing new concepts that could lead to breakthroughs in optical engineering have been proposed, and specific device designs have been introduced (particularly in the patent literature) on the basis of interpolating critical point energies as a function of composition. We note that the validity of these assumptions can only be verified by fabricating these new alloys as perfect substitutional crystals on conventional platforms that would allow a detailed and unambiguous characterization of their optoelectronic properties. While deposition chemistries needed to fabricate $Ge_{1-x}Si_x$ alloys are well understood and widely available corresponding protocols to introduce Sn into SiGe require the design of development of new process protocols based on chemically compatible sources. The facile reactivity of stannanes (hydrides of tin) over silane or germane derivatives extends the synthesis parameter space to unprecedented low-temperatures regimes which favor the formation of otherwise inaccessible compositions and metastable structures. In addition, the strong/large scattering cross section of Sn makes this element amenable to quantitative detection at very small concentrations (<1 at. %) in the lattice as well as routine and reliable spectroscopic analysis of the bonding and electronic properties.

The previously described advances in Ge and GeSn epitaxy and hydride precursors development have also enabled the CVD growth of $Ge_{1-x-y}Si_xSn_y (y = 2 - 12\%)$ ternaries with random diamond cubic structures [13]. Historically, these materials were initially deposited on GeSn and Ge buffered Si(100) via reactions of specifically designed Si–Ge–Sn hydrides described above such as SnD_4 and the $(H_3Ge)_x SiH_{4-x} (x = 1 - 4)$ family of silylgermanes. The latter furnish building blocks of specifically tailored elemental contents that possess the necessary reactivity to readily form the desired metastable $Ge_{1-x-y}Si_xSn_y$ structures and compositions at low temperatures (300–350 °C). For example, $(GeH_3)_2SiH_2$ reacts readily with SnD_4 at 350 °C to yield films with a Ge:Si ratio of 2 : 1, precisely matching that of the corresponding precursor. More recently, the routine growth of compositions containing up to 7 at. % Sn has been demonstrated on both Si(100) and Ge(100) wafers using commercially available sources such as trisilane, digermane, and stannane, thereby making the process suitable for direct industrial scale up and applications [20].

Extensive optical characterizations indicate that the properties of $Ge_{1-x-y}Si_xSn_y$ are independent of the platform on which they are grown including Si, Ge/Si(100) and GeSn/Si(100) and, most

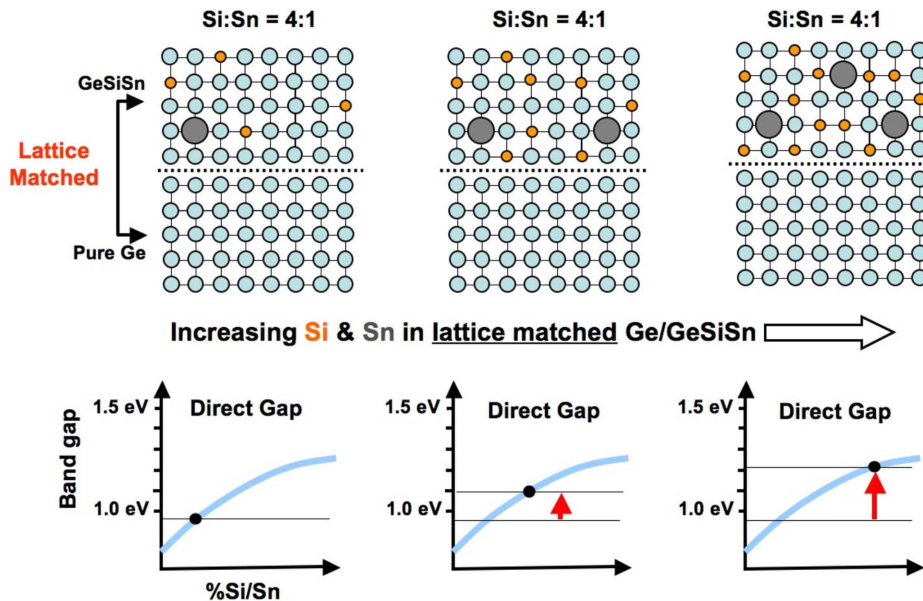

Fig. 9. Schematic illustration of the compositional tuning concept for Ge-rich SiGeSn alloys latticed matched to Ge (light blue circles), in which a ratio of Si (orange spheres) to Sn (large gray spheres) of 4 is maintained. The plots below illustrate the corresponding increase in band gap associated with the addition of Si and Sn, while preserving the 4 : 1 ratio.

recently, bulk Ge and GaAs substrates (see below for details concerning the latter platforms) [20]. More importantly, from an optoelectronic application perspective, the independent tuning of band gap and lattice constants has been unequivocally demonstrated for the first time in group-IV semiconductors [40]. In principle, alloy compositions can be generally chosen to lattice match a specific desired length scale ranging from that of Si to Sn. Experimentally, ternary alloys with Si to Sn molar ratio close to 4 : 1 possess a fixed lattice constant identical to that of Ge and can be routinely and reproducibly obtained for Si and Sn contents ranging from 2%–11% and 8%–43%, respectively [26], [41]. This is illustrated schematically in Fig. 9 which described the qualitative variation in the band gap (optical properties) of the ternary group IV films, whose molar volume and lattice constant remain unchanged as the composition of Si and Sn is increased. Accordingly, these materials can be viewed as "pseudobinary" alloys that can be described with a general formula $Ge_{1-X}(Si_{0.8}Sn_{0.2})_X$. The elemental composition of these systems is typically determined using RBS, as shown for a representative sample containing $\sim$10% Sn and $\sim$46% Si in the right panel of Fig. 10. Their optical properties of these alloys have been thoroughly measured, and plots containing the dependence of the direct gap (E_0) on composition X (left panel of Fig. 10) indicate that the corresponding transition energies are strongly nonlinear (e.g., large bowing) [40]. Nevertheless, the data show that the lowest direct gap E_0 increases monotonically as the Ge atoms are substituted by $Si_{0.8}Sn_{0.2}$ in the alloy, yielding a new family of semiconductors with properties complementary to those of SiGe and Ge. This makes it possible to design new optoelectronic devices fully compatible with Si processing that range from communication applications to sustainable energy systems such as photovoltaics based on hybrid group IV/III-V multijunctions. In the latter case the efficiency of the conventional Ge/InGaAs/InGaP designs is increased by inserting a material with the same lattice constant as Ge and a band gap close to 1 eV [42]–[44], as illustrated schematically in Fig. 11. In this context, the X minimum of the conduction band for SiGeSn should remain close to 1 eV (it is 1.1 eV in Si, and 0.9 eV in Ge and a-Sn), whereas the Γ (direct) and L minima increase as the Ge concentration is reduced while keeping the lattice constant equal to that of Ge. Thus, it may be possible to design an SiGeSn alloy where either all gaps or at least the direct and indirect (X) gaps are close to 1 eV, as required to improve solar cell performance. Finally, systematic doping protocols have been developed to produce *n* and *p-type* layers with Sn concentrations of 2, 5, and 8 at.% possessing remarkably high carrier mobilities

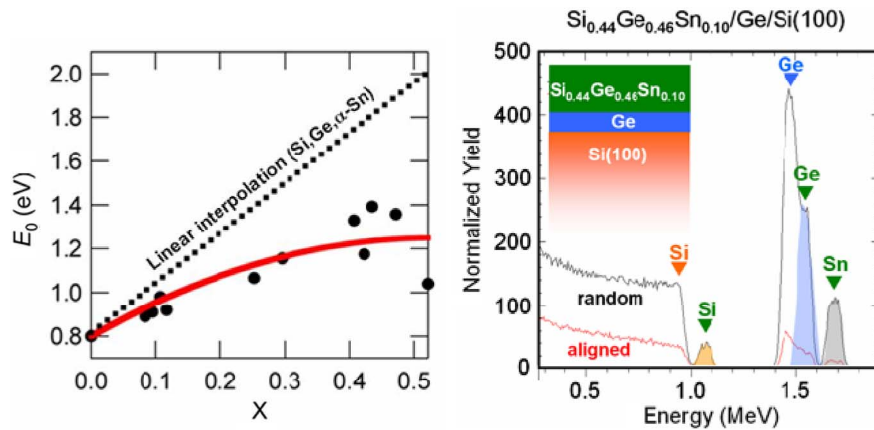

Fig. 10. (Left) Direct gap E_0 versus (Si+Sn) fraction X for $Ge_{1-X}(Si_{0.8}Sn_{0.2})_X$ alloys. The solid red line represents the best fit of the data, indicating that the gap reaches a maximum value and then decreases [42]. (Right) RBS spectrum of a representative Ge-lattice-matched sample showing distinct Si, Ge, and Sn signals from the atoms in the epilayer (green) and the buffer (blue). The aligned spectrum (red trace) indicates complete substitutionality of the Si, Ge, and Sn in the lattice.

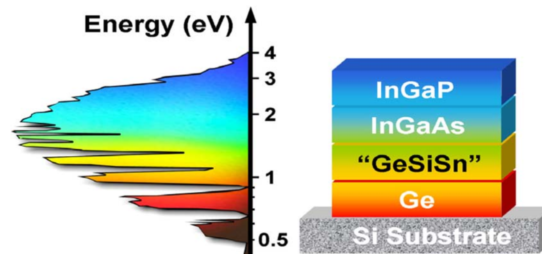

Fig. 11. Possible multijunction structures incorporating a lattice matched $Ge_{1-x}(Si_{0.8}Sn_{0.2})_X$ alloy (indicated as "SiGeSn") with bandgap of 1 eV.

comparable with those in elemental Ge, indicating that all elements are now in place to fabricate the first *PN* and *PIN* diodes based on these materials [45].

2.4. First Principles Simulation Studies

We also routinely integrate modern state-of-the-art simulations into our studies in order to elucidate the structural, optical, vibrational, thermoelastic, and thermodynamic behavior of group IV systems being investigated experimentally. Here, we focus on several key issues involving the role of atomic level distribution on the optical bandgap in ternaries lattice matched to Ge. For an ideal SiGeSn ternary alloy, statistical mechanics delivers the bond distributions which are in turn needed to describe the compositional dependence of the optical and vibrational properties. Cluster expansion models based on the Connolly-Williams approach [46] are used to estimate the properties of complex alloys by examining a finite number of discrete compositional configurations. We have successfully used this approach in prior work to predict the observed bandgap-composition dependence in SiCAlN quaternary alloys [6].

For SiGeSn systems containing significant concentrations of Sn, discrete quasi-random structural models can also be used to investigate the role of Sn nanoclusters on various properties of Si–Ge–Sn systems (e.g., thermoelastic, thermodynamic, optical). Our recent work on $Si_{1-x}Sn_x$ alloys, which represent the "SiSn" component of the SiGeSn ternary, has shown that nanoscale tuning of the Sn distribution within the alloy can have a profound effect on the value of the band gap for a given Sn content [47], and suggests that individual Bloch-like bands can be coaxed into the band

gap to potentially produce *bona fide* intermediate band (IB) photovoltaic materials. Accordingly, in the present work we investigate the effect of Sn atom clustering on optical properties of the SiGeSn alloys by explicit comparison of the band structure of random systems containing both *ideal* and *nonideal* bond distributions. Following our earlier work, we use density functional theory (DFT) as implemented in the VASP code [48], [49], and adopt random 64-atom supercells in which both atom positions and cell parameters are fully relaxed. In the case of ideal random alloys the atomic constituents are arbitrarily distributed on the available lattice sites to produce a series of compositions which are then screened on the basis of their bond distributions. Three configurations possessing the ideal alloy distributions (e.g., for a binary AB alloy $N_{AA} = x^2$, $N_{AB} = 2x(1-x)$, $N_{BB} = (1-x)^2$) are selected for subsequent calculation and the alloy properties are then simply obtained by averaging over these three distributions. We have verified that the averaged total electronic energies and molar volumes obtained using this procedure are essentially indistinguishable from those calculated using smaller 32-atom special quasi-random structures (SQS) at a number of compositions (0.125, 0.25) [50].

In the present case of the Ge-lattice-matched systems, we also adopt a 64-atom cell representation with random distributions of Si, Ge and Sn atoms. Among the configurations explored we specifically retain those which possess ideal bond distributions obtained from simple concentration products of the corresponding elemental constituents at each composition. For example the number of homonuclear Sn-Sn bonds is x^2 while for the heteronuclear Sn-Ge and Ge-Sn analogs the total is $x(1-5x) + (1-5x)x = 2x(1-5x)$. Here, again, fundamental alloy properties such as energies and lattice constants are obtained by averaging over the three selected configurations. For the purpose of describing the bonding within these configurations, it is convenient to express the Ge-matched ternary as a pseudo-binary admixture of pure Ge and $Si_{0.8}Sn_{0.2}$, where the latter is a random alloy possessing the Ge lattice constant. By defining $X = 1 - 5x$, this can be written with a general formula of $Ge_{1-X}(Si_{0.8}Sn_{0.2})_X$, where X represents the Ge content in the material. The corresponding "ideal" bond distributions for this system are plotted as a function of composition in Fig. 12, which elucidates distinct bonding regimes exhibiting SiSn-like ($X \sim 1$), SiGe-like ($X \sim 0.25$) and Ge-like ($X \sim 0$) behavior are expected. It is interesting to note the SiGe-like regime corresponds to alloys with 5%–8% Sn content, which are observed to exhibit facile formation and a remarkable thermal stability in spite of their high Sn content, as discussed in recent work describing the thermodynamics of these systems [26].

The electronic energies of the random alloys are obtained directly from the VASP code from a full structural optimization over the cell parameters (zero stress) and all atomic positions (zero force). We employed the Ceperley-Alder parameterization of the local density functional (CA-LDA) [51], [52], a plane wave cutoff of 350 eV, and a $3 \times 3 \times 3$ Monkhorst-Pack sampling for reciprocal space integrations yielding 14 irreducible *k*-points in the first Brillouin zone. Using these computational conditions we obtained the electronic ground state energy and relaxed structures of nine compositions in the range from 0% to 13% Sn, by averaging over three configurations in each case, as described earlier.

A by-product of the latter calculations is the band structure of the ternary alloys. To compute the band energies, we evaluated the electronic density using a denser grid of *k*-points (approximately 55 irreducible points) and the optimized atomic structures for each composition. The electronic energies were then evaluated along a series of standard paths in the Brillouin zone corresponding to our simple cubic supercell. The resulting band gaps were found to vary from 0.0 to approximately 0.3 eV as the Ge content was reduced [e.g., increasing the percent amount of $(Si_{0.8}Sn_{0.2})$]. The vanishing of the band gap for Ge is a well-known limitation of the LDA so that the results obtained here provide quantitative trends only with respect to the compositional variation rather than the absolute value of the gaps. The actual values of the band gap were found to vary by less than 0.02 eV between random configurations for a given composition, justifying the use of a simple arithmetic average. For the Ge-rich systems considered here a simple shift (offset) of the calculated band gaps by the observed value of 0.78 eV was applied as shown in the vertical axis of Fig. 12. Over the range of Sn concentrations form ~5%–10%, this fixed shift gives essentially the same values as the Vegard average of the corrections for Si (~0.62 eV), Ge (~0.78 eV) and Sn (0 eV). The plot in Fig. 13(a), which

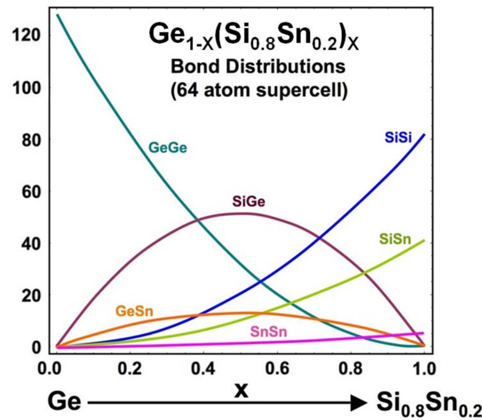

Fig. 12. Ge concentration dependence of the statistical bond distributions in ideal $Ge_{1-X}(Si_{0.8}Sn_{0.2})_X$ alloys possessing the lattice constant of pure Ge, where $1 - X = 5x$ represent the fraction of Ge in the ternary. The vertical axis is normalized to the *maximum* number of bonds (128) in a 64-atom diamond lattice supercell.

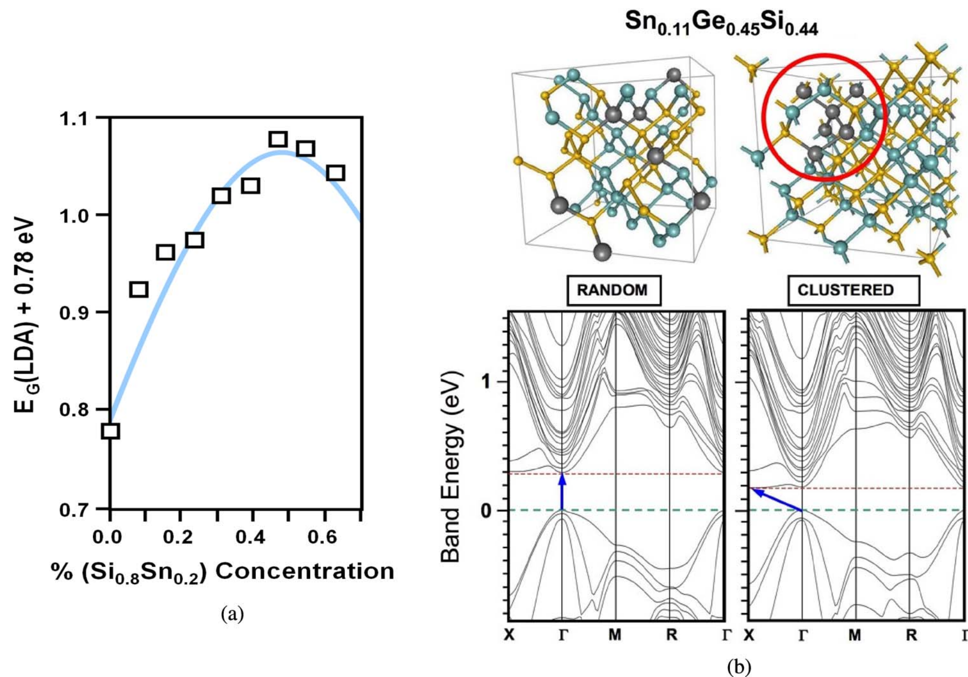

Fig. 13. (a) LDA band gap dependence on $\%(Si_{0.8}Sn_{0.2})$ indicating a gradual increase of the gap to a maximum value of 1.08 eV for $Si_{0.44}Ge_{0.45}Sn_{0.11}$. (b) LDA electronic band structure in the vicinity of the band gap for a representative $Si_{0.44}Ge_{0.45}Sn_{0.11}$ alloy with Si/Sn ratio of 4, in which the Sn atoms are randomly distributed (left) or clustered (right). In this example, the Sn clustering reduces the gap by 50% and alters the character of the transition from $\Gamma \rightarrow \Gamma$ to $\Gamma \rightarrow X$ (Note that the *k*-space points refer to a simple cubic supercell and not the traditional FCC primitive cell.) Legend: Silicon (yellow), Germanium (blue), Tin (gray).

includes these corrections, indicates a systematic increase in the band gap with Si and Sn concentration up a maximum value of ~1.1 eV for an alloy with composition $Ge_{0.45}Si_{0.44}Sn_{0.11}$, followed by a small decrease for larger concentrations of Si/Sn, in semiquantitative agreement with the experimental results presented in Fig. 10.

A potential concern in SiSnGe ternary alloys is clustering of the Sn atoms on the nanoscale, particularly in samples with high Sn concentrations. As mentioned above, this may have a profound

effect on key thermoelastic, thermodynamic, and optical properties. Here, we briefly investigate the impact of Sn clustering on the band-structure by constructing a series of unit cell configurations with a common composition but Sn-Sn bonding distributions that are intentionally enhanced relative to the ideal random case. This is illustrated in Fig. 13(b) for the $Si_{0.44}Ge_{0.45}Sn_{0.11}$ alloy for which Sn-clustering is seen to reduce the band gap by 50% over random alloys which typically contain only $\sim$1.6% Sn-Sn bonds (Note that in an ideal 64-atom random alloy representation of $Si_{0.8}Sn_{0.2}$, there are 82 Si-Si bonds, 41 Si-Sn bonds, and only five Sn-Sn bonds.) Furthermore, the band plots in the figure clearly indicate that the character of the transitions is profoundly altered by the clustering of Sn, exhibiting an apparent change from a direct gap to an indirect gap semiconductor. A more precise determination of the symmetry of the valence band (VB) to conduction band (CB) transitions will require an analysis of the band folding from simple cubic to FCC.

2.5. Comparative Studies of SiGeSn on Ge and GaAs

To establish the generality of our synthesis and processing approach we also recently deposited Ge matched ternaries on both nonpolar Ge and polar GaAs bulk wafers. The latter substrates were specifically chosen since they are commonly used in commercial multijunction solar cells, including the recently introduced "inverted design," in which the ordering of the junctions is reversed relative to the conventional architectures. The objective here is to show that using similar deposition protocols the materials can be integrated onto these non-Si bulk substrates. The insertion of SiGeSn layers into current three junction structures will likely extend the capability of these conventional devices by increasing their efficiency.

The growth procedure involved the typical wafer pre-deposition cleaning steps, including rinsing in HF/methanol solutions followed by drying in a N_2 stream. The substrates were subsequently transferred into the reactor and heated to a nominal growth temperature of 350–375 °C. In both cases, high-purity digermane diluted in H_2 was allowed to flow over the wafer surface for 2 min at 10^{-4} Torr for the purpose of removing any residual surface contaminants prior to commencing the growth of the bulk layer. This was an enabling step to ensure successful formation of monocrystalline and epitaxial samples under these low-temperature conditions employed in these experiments. Under these conditions, layers with defect-free and fully commensurate interfaces were produced at typical growth rates of 10–15 nm/min. Fig. 14 shows representative XTEM, XRD, and RBS plots for the SiGeSn films obtained on bulk Ge and GaAs wafers. The XTEM image shows that a 250-nm-thick layer of Ge-matched $Ge_{0.90}Si_{0.08}Sn_{0.02}$ is devoid of threading dislocations and possesses an atomically flat surface when grown directly on a bulk Ge wafer. The reciprocal space map in part (b) of the figure shows that the Ge/SiGeSn heterostructure is fully relaxed and perfectly lattice matched. In contrast, the $\omega/2\theta$ plot in part (c) shows that the same composition of SiGeSn grown directly on a bulk GaAs wafer is slightly mismatched with the underlying substrate as expected. The XRD plot contains two distinct (004) peaks corresponding to the epilayer and the underlying wafer. This data also show the characteristic fringe pattern due to the minor lattice mismatch and the finite thickness of the film. This feature is also indicative of the high quality of these film in terms of thickness uniformity, smooth and abrupt interface, flat surface, and low defect density of the bulk. RBS plots of the latter sample, such as those shown in Fig. 14(d), provide the nominal layer thickness and the elemental composition of the samples. The aligned RBS give a semiquantitative assessment of the epitaxial registry between the film and the wafer, as well as the substitionality of the Si, Ge, and Sn constituents in the diamond cubic framework.

3. Summary

New families of molecular hydrides with tunable reactivities and compositions have been developed, and their applications in CVD synthesis of group-IV semiconductors, including alloys incorporating Sn, have been explored. Here, we have focused on the synthesis, materials properties, and device applications of three such Ge-based semiconductor systems fully integrated with Si including (1) Ge layers with thicknesses >5 mm possessing dislocation densities $<10^5/cm^2$ are formed below 400 °C by combining of Ge_2H_6 and highly reactive $(GeH_3)_2CH_2$ organometallic additives circumventing the

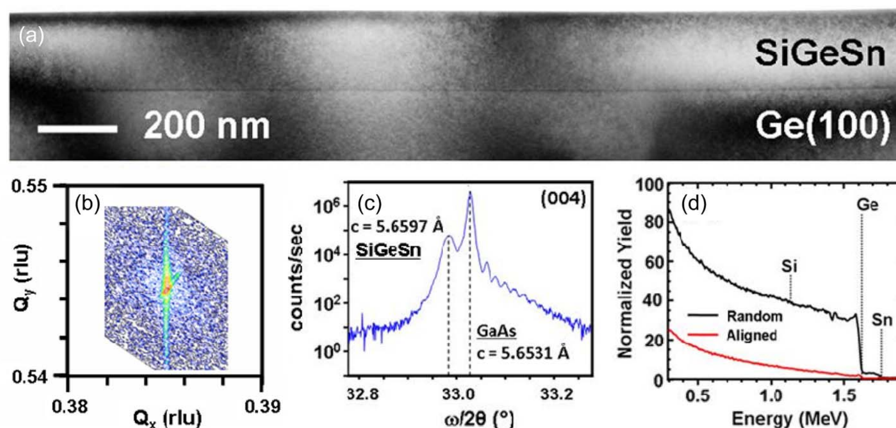

Fig. 14. (a) XTEM micrograph of $Ge_{0.90}Si_{0.08}Sn_{0.02}$ grown on a bulk Ge indicating that the layer is flat and devoid of threading defects. (b) Reciprocal space map of the (004) reflection showing in-plane lattice matching of the epilayer with Ge platform. (c) XRD plots of SiGeSn layers grown on GaAs(100) wafers showing clearly resolved peaks from the epilayer and the substrate. The presence of interference fringes indicates a high degree of crystallinity and epitaxial alignment between the slightly mismatched (0.1%) materials. (d) RBS random and channeled spectra of the entire heterostructure showing distinct signals from the Si, Ge, and Sn in the epilayer superimposed upon the dominant GaAs background. The epitaxial commensuration is corroborated by the near perfect channeling (red trace).

classical Stranski-Krastanov growth mechanism; (2) GeSn alloys are grown via reactions of Ge_2H_6 and SnD_4; and (3) ternary SiGeSn analogs are produced lattice-matched to Ge-buffered Si using admixtures of commercially viable $SiGeH_6$, SnD_4, Ge_2H_6, and Si_3H_8 sources. Optical experiments demonstrate that the SiGeSn system represents the first group-IV alloy with a tunable electronic structure at fixed lattice constant, effectively decoupling band gap and strain and eliminating the most important limitation for device designs in this class of materials. From a device perspective, doping levels of 10^{19} cm^{-3} are routinely achievable in all the above systems using chemically and structurally compatible $P(SiH_3)_3$ and (P, As)$(GeH_3)_3$ delivery agents. Applications of Ge-Sn materials in the fabrication of high performance, near IR photodiodes have been demonstrated. The results show that the binaries significantly expand the range of detection beyond that of Ge (1550 nm) and substantially increase the absorption, indicating that these materials represent a viable alternative to Ge in IR photonic applications, including high-performance detectors and photovoltaics.

References

[1] S. Aldridge and A. J. Downs, "Hydrides of the main-group metals: New variations on an old theme," *Chem. Rev.*, vol. 101, no. 11, pp. 3305–3366, Nov. 2001.
[2] J. A. Jegier and W. L. Gladfelter, "The use of aluminum and gallium hydrides in materials science," *Coordination Chem. Rev.*, vol. 206/207, pp. 631–650, Sep. 2000.
[3] J. McMurran, J. Kouvetakis, D. Nesting, D. Smith, and J. L. Hubbard, "Formation of a tetrameric, cyclooctane-like, azidochlorogallane $[HClGaN_3]_4$, and related azidogallanes. Exothermic single-source precursors to GaN nanostructures," *J. Amer. Chem. Soc.*, vol. 120, no. 21, pp. 5233–5237, Jun. 1998.
[4] J. McMurran, D. Dai, K. Balasubramanian, C. Steffek, J. Kouvetakis, and J. L. Hubbard, "H_2GaN_3 and derivatives: A facile method to gallium nitride," *Inorg. Chem.*, vol. 37, no. 26, pp. 6638–6644, Dec. 1998.
[5] R. A. Trivedi, J. Tolle, A. V. G. Chizmeshya, R. Roucka, C. Ritter, J. Kouvetakis, and I. S. T. Tsong, "Low-temperature GaN growth on silicon substrates by single gas-source epitaxy and photo-excitation," *Appl. Phys. Lett.*, vol. 87, no. 7, p. 072 107, Aug. 2005.
[6] R. Roucka, J. Tolle, A. V. G. Chizmeshya, P. A. Crozier, C. D. Poweleit, D. J. Smith, I. S. T. Tsong, and J. Kouvetakis, "Low-temperature epitaxial growth of the quaternary wide band gap semiconductors SiCAlN," *Phys. Rev. Lett.*, vol. 88, no. 20, p. 206 102/1, May 2002.
[7] L. Torrison, J. Tolle, D. J. Smith, C. Poweleit, J. Menendez, M. M. Mitan, T. L. Alford, and J. Kouvetakis, "Morphological and optical properties of Si nanostructures imbedded in SiO_2 and Si_3N_4 films grown by single source CVD," *J. Appl. Phys.*, vol. 92, no. 12, pp. 7475–7480, Dec. 2002.
[8] J. B. Tice, V. R. D'Costa, G. Grzybowski, A. V. G. Chizmeshya, J. Tolle, J. Menendez, and J. Kouvetakis, "Synthesis and optical properties of amorphous $Si_3N_{4-x}P_x$ dielectrics and complementary insights from *ab initio* structural simulation," *Chem. Mater.*, vol. 22, no. 18, pp. 5296–5305, Sep. 2010.

[9] R. Trivedi, P. L. Liu, R. Roucka, J. Tolle, A. V. G. Chizmeshya, I. S. T. Tsong, and J. Kouvetakis, "Mismatched heteroepitaxy of tetrahedral semiconductors with Si via ZrB_2 templates," *Chem. Mater.*, vol. 17, no. 18, pp. 4647–4652, Sep. 2005.

[10] A. V. G. Chizmeshya, C. Ritter, J. Tolle, C. Cook, J. Menendez, and J. Kouvetakis, "Fundamental studies of $P(GeH_3)_3$, $As(GeH_3)_3$, and $Sb(GeH_3)_3$: Practical *n*-dopants for new group IV semiconductors," *Chem. Mater.*, vol. 18, no. 26, pp. 6266–6277, Dec. 2006.

[11] J. Kouvetakis, A. Haaland, D. J. Shorokhov, H. V. Volden, G. V. Girichev, V. I. Sokolov, and P. Matsunaga, "Novel methods for CVD of Ge_4C and $(Ge_4C)_xSi_y$ diamond-like semiconductor heterostructures: Synthetic pathways and structures of trigermyl-$(GeH_3)_3CH$ and tetragermyl-$(GeH_3)_4C$ methanes," *J. Amer. Chem. Soc.*, vol. 120, no. 27, pp. 6738–6744, Jul. 1998.

[12] J. Kouvetakis, D. Chandrasekhar, and D. J. Smith, "Growth and characterization of thin $Si_{80}C_{20}$ films based upon Si_4C building blocks," *Appl. Phys. Lett.*, vol. 72, no. 8, pp. 930–932, Feb. 1998.

[13] J. Kouvetakis and A. V. G. Chizmeshya, "New classes of Si-based photonic materials and device architectures via designer molecular routes," *J. Mater. Chem.*, vol. 17, pp. 1649–1655, 2007.

[14] C. J. Ritter, C. Hu, A. V. G. Chizmeshya, J. Tolle, D. Klewer, I. S. T. Tsong, and J. Kouvetakis, "Synthesis and fundamental studies of $(H_3Ge)_xSiH_{4-x}$ molecules: Precursors to semiconductor hetero- and nanostructures on Si," *J. Amer. Chem. Soc.*, vol. 127, no. 27, pp. 9855–9864, Jul. 2005.

[15] A. V. G. Chizmeshya, C. Ritter, C. Hu, J. Tolle, R. Nieman, I. Tsong, and J. Kouvetakis, "Synthesis of butane-like Si-Ge hydrides: Enabling precursors for CVD of Ge-rich semiconductors," *J. Amer. Chem. Soc.*, vol. 128, no. 21, pp. 6919–6930, May 2006.

[16] J. B. Tice, A. V. G. Chizmeshya, R. Roucka, J. Tolle, B. R. Cherry, and J. Kouvetakis, "$Cl_nH_{6-n}SiGe$ compounds for CMOS compatible semiconductor applications: Synthesis and fundamental studies," *J. Amer. Chem. Soc.*, vol. 129, no. 25, pp. 7950–7960, Jun. 2007.

[17] J. Tolle, R. Roucka, A. V. G. Chizmeshya, J. Kouvetakis, V. R. D'Costa, and J. Menendez, "Compliant tin-based buffers for the growth of defect-free strained heterostructures on silicon," *Appl. Phys. Lett.*, vol. 88, no. 25, p. 252 112, Jun. 2006.

[18] V. R. D'Costa, C. S. Cook, A. G. Birdwell, C. L. Littler, M. Canonico, S. Zollner, J. Kouvetakis, and J. Menendez, "Optical critical points of thin-film $Ge_{1-y}Sn_y$ alloys: A comparative $Ge_{1-y}Sn_y/Ge_{1-x}Si_x$ study," *Phys. Rev. B, Condens. Matter*, vol. 73, no. 12, p. 125 207, Mar. 2006.

[19] M. Bauer, J. Taraci, J. Tolle, A. V. G. Chizmeshya, S. Zollner, D. J. Smith, J. Menendez, C. Hu, and J. Kouvetakis, "Ge-Sn semiconductors for band-gap and lattice engineering," *Appl. Phys. Lett.*, vol. 81, no. 16, pp. 2992–2994, Oct. 2002.

[20] J. Xie, A. V. G. Chizmeshya, J. Tolle, V. R. D'Costa, J. Menendez, and J. Kouvetakis, "Synthesis, stability range and fundamental properties of Si-Ge-Sn semiconductors grown directly on large area Si(100) and Ge(100) platforms," *Chem. Mater.*, vol. 22, no. 12, pp. 3779–3789, Jun. 2010.

[21] M. A. Wistey, Y. Y. Fang, J. Tolle, A. V. G. Chizmeshya, and J. Kouvetakis, "Chemical routes to Ge/Si(100) structures for low temperature Si-based semiconductor applications," *Appl. Phys. Lett.*, vol. 90, no. 8, p. 082 108, Feb. 2007.

[22] R. Soref, "The past, present, and future of silicon photonics," *IEEE J. Sel. Topics Quantum Electron.*, vol. 12, no. 6, pp. 1678–1687, Nov./Dec. 2006.

[23] S. G. Thomas, M. Bauer, M. Stephens, C. Ritter, and J. Kouvetakis, "Precursors for Group IV epitaxy for microelectronic and optoelectronic applications," *Solid State Technol.*, vol. 52, no. 4, pp. 12–15, 2009.

[24] J. B. Tice, Y.-Y. Fang, J. Tolle, A. V. G. Chizmeshya, and J. Kouvetakis, "Synthesis and fundamental studies of chlorinated Si-Ge hydride macromolecules for strain engineering and selective-area epitaxial applications," *Chem. Mater.*, vol. 20, no. 13, pp. 4374–4385, Jul. 2008.

[25] J. B. Tice, A. V. G. Chizmeshya, J. Tolle, V. R. D'Costa, J. Menendez, and J. Kouvetakis, "Practical routes to $(SiH_3)_3P$: Applications in group IV semiconductor activation and in group III–V molecular synthesis," *Dalton Trans.*, vol. 39, no. 19, pp. 4551–4558, 2010.

[26] J. Xie, J. Tolle, V. R. D'Costa, A. V. G. Chizmeshya, J. Menendez, and J. Kouvetakis, "Direct integration of active $Ge_{1-x}(Si_4Sn)_x$ semiconductors on Si(100)," *Appl. Phys. Lett.*, vol. 95, no. 18, p. 181 909, Nov. 2009.

[27] J. Xie, J. Tolle, V. R. D'Costa, C. Weng, A. V. G. Chizmeshya, J. Menendez, and J. Kouvetakis, "Molecular approaches to *p*- and *n*-nanoscale doping of $Ge_{1-y}Sn_y$ semiconductors: Structural, electrical and transport properties," *Solid State Electron.*, vol. 53, no. 8, pp. 816–823, Aug. 2009.

[28] M. Yang, M. Carroll, J. C. Sturm, and T. J. Buyuklimanli, "Phosphorus doping and sharp profiles in silicon and silicon-germanium epitaxy by rapid thermal chemical vapor deposition," *J. Electrochem. Soc.*, vol. 147, no. 9, pp. 3541–3545, 2000.

[29] K. D. Hobart, F. J. Kub, G. G. Jernigan, and P. E. J. Thompson, "Surface segregation of arsenic and phosphorus from buried layers during Si molecular beam epitaxy," *J. Vac. Sci. Technol. B, Microelectron. Nanometer Struct.*, vol. 14, no. 3, pp. 2229–2232, May 1996.

[30] M. Racanelli and D. W. Greve, "In situ doping of Si and $Si_{1-x}Ge_x$ in ultra-high vacuum chemical vapor deposition," *J. Vac. Sci. Technol. B, Microelectron. Nanometer Struct.*, vol. 9, no. 4, pp. 2017–2021, Jul. 1991.

[31] Y.-H. Kuo, Y. K. Lee, K. Yong, Y. Ge, S. Ren, J. E. Roth, T. I. Kamins, D. A. B. Miller, and J. S. Harris, "Strong quantum-confined Stark effect in germanium quantum-well structures on silicon," *Nature*, vol. 437, no. 7063, pp. 1334–1336, Oct. 2005.

[32] J. Mathews, R. Roucka, J. Xie, S.-Q. Yu, J. Menendez, and J. Kouvetakis, "Extended performance GeSn/Si(100) p-i-n photodetectors for full spectral range telecommunication applications," *Appl. Phys. Lett.*, vol. 95, no. 13, pp. 133506/1–133506/3, Sep. 2009.

[33] J. Kouvetakis, J. Menendez, and A. V. G. Chizmeshya, "Sn-based group-IV semiconductors: A new platform for opto- and microelectronics on Si," *Annu. Rev. Mater. Res.*, vol. 36, pp. 497–554, 2006.

[34] R. Roucka, J. Mathews, C. Weng, R. Beeler, J. Tolle, J. Menendez, and J. Kouvetakis, "Extended performance of GeSn p-i-n photodiodes," *J. Quantum Electron.*, under review.

[35] Y.-Y. Fang, J. Tolle, V. D'Costa, J. Menendez, A. V. G Chizmeshya, and J. Kouvetakis, "Epitaxy-driven synthesis of elemental Ge/Si strain-engineered materials and device structures via designer molecular chemistry," *Chem. Mater.*, vol. 19, no. 24, pp. 5910–5925, Nov. 2007.

[36] L. Colace and G. Assanto, “Germanium on silicon for near-infrared light sensing,” *IEEE Photon. J.*, vol. 1, no. 2, pp. 69–79, Aug. 2009.
[37] C. Auth, M. Buehler, A. Cappellani, C. Choi, G. Ding, W. Han, S. Joshi, B. McIntyre, M. Prince, P. Ranade, J. Sanford, and C. Thomas, “45 nm high-k+metal gate strain-enhanced transistors,” *Intel Technol. J.*, vol. 12, no. 2, pp. 77–86, 2008.
[38] B. Jalali, M. Paniccia, and G. Reed, “Silicon photonics,” *IEEE Microw. Mag.*, vol. 7, p. 1440, 2006.
[39] T. Ghani, M. Armstrong, C. Auth, M. Bost, P. Charvat, G. Glass, T. Hoffmann, K. Johnson, C. Kenyon, J. Klaus, B. McIntyre, K. Mistry, A. Murthy, J. Sandford, M. Silberstein, S. Sivakumar, P. Smith, K. Zawadzki, S. Thompson, and M. Bohr, “A 90 nm high volume manufacturing logic technology featuring novel 45 nm gate length strained silicon CMOS transistors,” in *IEDM Tech. Dig.*, 2003, pp. 978–980.
[40] V. R. D’Costa, Y.-Y. Fang, J. Tolle, J. Kouvetakis, and J. Menendez, “Tunable optical gap at a fixed lattice constant in Group-IV semiconductor alloys,” *Phys. Rev. Lett.*, vol. 102, no. 10, pp. 107 403/1–107 403/4, Mar. 2009.
[41] Y.-Y. Fang, J. Xie, J. Tolle, R. Roucka, V. R. D’Costa, A. V. G. Chizmeshya, J. Menendez, and J. Kouvetakis, “Molecular-based synthetic approach to new group IV materials for high-efficiency, low-cost solar cells and Si-based optoelectronics,” *J. Amer. Chem. Soc.*, vol. 130, no. 47, pp. 16 095–16 102, Nov. 2008.
[42] F. Dimroth and S. Kurtz, “High-efficiency multijunction solar cells,” *MRS Bull.*, vol. 32, p. 230, 2007.
[43] D. J. Friedman, S. R. Kurtz, and J. F. Geisz, “Analysis of the GaInP/GaAs/1-eV/Ge cell and related structures for terrestrial concentrator application,” in *Conf. Rec. 29th IEEE Photovolt. Spec. Conf.*, 2002, pp. 856–859.
[44] D. C. Senft, “Progress in crystalline multijunction and thin-film photovoltaics,” *J. Electron. Mater.*, vol. 34, no. 5, pp. 571–574, May 2005.
[45] Y. Y. Fang, J. Tolle, V. R. D’Costa, A. V. G. Chizmeshya, J. Menendez, and J. Kouvetakis, “Practical B and P doping via $Si_xSn_yGe_{1-x-y-z}M_z$ quaternaries lattice matched to Ge: Structural, electrical and strain behavior,” *Appl. Phys. Lett.*, vol. 95, no. 8, p. 081 113, Aug. 2009.
[46] J. D. D. Connolly and A. R. Williams, “Density-functional theory applied to phase transformations in transition-metal alloy,” *Phys. Rev. B, Condens. Matter*, vol. 27, no. 8, pp. 5169–5172, Apr. 1983.
[47] J. Tolle, A. V. G. Chizmeshya, Y. Y. Fang, J. Kouvetakis, V. R. D. Costa, C. W. Hu, J. Menendez, and I. S. T. Tsong, “Low temperature chemical vapor deposition of Si-based compounds via $[SiH_3SiH_2SiH_3]$: Metastable SiSn/GeSn/Si(100) heteroepitaxial structures,” *Appl. Phys. Lett.*, vol. 89, no. 23, p. 231 924, Dec. 2006.
[48] G. Kresse and J. Furthmuller, “Efficient iterative schemes for *ab initio* total-energy calculations using a plane-wave basis set,” *Phys. Rev. B, Condens. Matter*, vol. 54, no. 16, pp. 11 169–11 186, Oct. 1996.
[49] G. Kresse and J. Hafner, “Norm-conserving and ultrasoft pseudopotentials for first-row and transition-elements,” *J. Phys. Condens. Matter*, vol. 6, no. 40, pp. 8245–8257, Oct. 1994.
[50] A. Chroneos, C. Jiang, R. W. Grimes, U. Schwingenschlogl, and H. Bracht, “E centers in ternary $Si_{1-x-y}Ge_xSn_y$ random alloys,” *Appl. Phys. Lett.*, vol. 95, no. 11, p. 112 101, Sep. 2009.
[51] D. M. Ceperley and B. J. Alder, “Ground state of the electron gas by a stochastic method,” *Phys. Rev. Lett.*, vol. 45, no. 7, pp. 566–569, Aug. 1980.
[52] J. P. Perdew and A. Zunger, “Self-interaction correction to density-functional approximations for many-electron systems,” *Phys. Rev. B, Condens. Matter*, vol. 23, no. 10, pp. 5048–5079, May 1981.